www.czasopisma.pan.pl PAN POLSKA AKADEMIA NAUK www.journals.pan.pl

Arch. Min. Sci. **64** (2019), 3, 609-623

Electronic version (in color) of this paper is available: http://mining.archives.pl

DOI 10.24425/ams.2019.129372

DAWEI YIN*, SHAOJIE CHEN*#, BING CHEN*, ZHIGUO XIA*

SIMULATION STUDY ON STRENGTH AND FAILURE CHARACTERISTICS OF COAL-ROCK COMPOSITE SAMPLE WITH COAL PERSISTENT JOINT

BADANIE SYMULACYJNE CHARAKTERYSTYK WYTRZYMAŁOŚCIOWYCH PRÓBKI KOMPOZYTOWEJ ZŁOŻONEJ Z MATERIAŁU SKALNEGO ORAZ WĘGLA W KTÓRYM WYSTĘPUJĄ PŁASZCZYZNY ŁUPLIWOŚCI

Dynamic Mine disasters can be induced by the instability and failure of a composite structure of rock and coal layers during coal mining. Coal seam contains many native defects, severely affecting the instability and failure of the compound structure. In this study, the effects of coal persistent joint on the strength and failure characteristics of coal-rock composite samples were evaluated using PFC2D software. The results show that with the increase of included angle α between the loading direction and joint plane direction, the uniaxial compressive stress (UCS) and peak strain of composite samples first decrease and then gradually increase. The elastic moduli of composite samples do not change obviously with α. The peak strain at α of 45° is the lowest, and the UCS at α of 30° is the smallest. This is inconsistent with theoretical analysis of lowest UCS at α of 45°. This is because that the local stress concentration caused by the motion inconformity of composite samples may increase the average axial stress of upper wall in PFC2D software. Moreover, the coal persistent joint promotes the transformation from the unstable crack expansion to the macro-instability of composite samples, especially at α of 30° and 45°. The majority of failures for composite samples occur within the coal, and no obvious damage is observed in rock. Their failure modes are shear failure crossing or along the coal persistent joint. The failure of composite sample at α of 30° is a mixed failure, including the shear failure along the persistent joint in coal and tensile failure of rock induced by the propagation of coal persistent joint.

Keywords: particle flow simulation, coal-rock composite sample, coal persistent joint, strength and failure characteristics, microcrack number evolution

Niekorzystne zjawiska dynamiczne w kopalniach mogą być wywołane przez niestabilność i pękanie struktur kompozytowych złożonych z warstw węgla i materiałów skalnych w trakcie eksploatacji górniczej. W złożu węgla ujawnić się mogą liczne defekty wewnętrzne, które w poważnym stopniu rzutują na stabilność i wytrzymałość złożonej struktury. W pracy tej zbadano wpływ spoistości węglu (występowania powierzchni łupliwości) na charakterystykę wytrzymałościową próbki kompozytowej złożonej z węgla

* STATE KEY LABORATORY OF MINE DISASTER PREVENSION AND CONTROL, SHANDONG UNIVERSITY OF SCIENCE AND TECHNOLOGY, QINGDAO 266590, CHINA

Corresponding author: csjwyb@163.com

i skały z wykorzystaniem oprogramowania PCF 2D. Wyniki symulacji wskazują, że wraz ze wzrostem kąta α pomiędzy kierunkiem działania obciążenia a płaszczyzną łupliwości, jednoosiowe naprężenie ściskające oraz maksymalne odkształcenie próbki kompozytowej w pierwszym etapie zmniejszą się, a następnie zaczną stopniowo wzrastać. Moduł sprężystości próbek kompozytowych nie ulega zmianie wraz ze zmianą kąta α. Maksymalne odkształcenie będzie najmniejsze dla kąta α równego 45°, z kolei jednoosiowe naprężenie ściskające zarejestrowane dla 30° okaże się najniższe. Wyniki te nie wykazują zgodności z wynikami analiz teoretycznych, przewidujących iż najniższe wartości jednoosiowego naprężenia ściskającego powinny wystąpić dla kąta 45°. Dzieje się tak dlatego, że lokalne koncentracje naprężeń wskutek odmienności zachowania poszczególnych składników próbki w trakcie ruchu powodować mogą wzrost średniego naprężenia osiowego ściany górnej, co uwzględnia model z wykorzystaniem oprogramowania PFC 2D. Ponadto, istnienie ciosu i płaszczyzn łupliwości sprawia, że niestabilne i propagujące szczeliny ulegają przekształceniu w makro- niestabilności próbek kompozytowych, zwłaszcza przy kącie α równym 30° i 45°. Większość pęknięć powstających w próbkach kompozytowych występuje w części węglowej, w pozostałych skałach nie notuje się poważniejszych uszkodzeń. Pęknięcia zmęczeniowe w części złożonej z materiału skalnego odbywają się wskutek działania naprężeń ścinających wzdłuż lub w poprzez płaszczyzny łupliwości. Pękanie zmęczeniowe próbki kompozytowej przy kącie α równym 30° jest procesem złożonym, obejmującym pękanie wskutek naprężeń ścinających działających wzdłuż płaszczyzny łupliwości w węglu oraz naprężeń rozciągających działających na część próbki złożoną z materiału skalnego, wskutek propagacji pęknięcia.

Słowa kluczowe: symulacja PFC, próbką kompozytowa złożona z węgla i materiału skalnego, spoistość węgla, charakterystyka wytrzymałościowa, ewolucja mikro- pęknięć

1. Introduction

Many dynamic hazards frequently occur in the process of coal mining, such as the rock burst, coal and gas outburst, etc., severely threatening the safe production of coal mine (Hauquin et al., 2018; Espinoza et al., 2015; Liu et al., 2019; Li et al., 2018). The rock of underground mining in colliery is layered stratum formed by sedimentation (Huang & Liu, 2013; Bao et al., 2013), and dynamic hazards can be caused by the instability and failure of a composite structure of roof or floor rock and coal layers under the effects of mining disturbance (Lu et al., 2015; Lama & Bodziony, 1998; Paul et al., 2012; Petukhov & Linkov, 1979; Zhao et al., 2016). Rock burst hazard can be induced by the fall of hard roof (Lu et al., 2015; Snelling et al., 2013; Chen et al. 2019). Therefore, it is essential to study the strength and failure characteristics of the composite structure of rock and coal layers.

There are three types of composite structures of rock and coal layers, including the roof rock-coal composite structure, coal-floor rock composite structure, and roof rock-coal-floor rock composite structure, as shown in Fig. 1. Under mining disturbance, any instability and failure in either of the three types of composite structures can lead to dynamic hazards in mining.

To evaluate the strength and failure characteristics of composite structures of rock and coal layers, the different interbedded modes of coal and rock layers in a coal mine are simplified as a composite sample consisting of coal and rock in the laboratory tests or numerical simulation tests. Petukhov and Linkov (1979) analyzed the stability of general bipartite system and rock-coal system while studying the stable behavior of rock mass after post-peak point. Poulsen et al. (2014) studied the strength reduction of a coal pillar due to water saturation embedded in roof rock-coal pillar-floor rock combined body. Chen et al. (2017) found that with the increase of the height ratio of rock to coal, the uniaxial compressive stress (UCS), macrofailure initiation stress and elastic modulus of a rock-coal composite sample decreased. The effects of uniaxial loading rates on the strength of a roof sandstone-coal composite sample were studied by Yin et al.

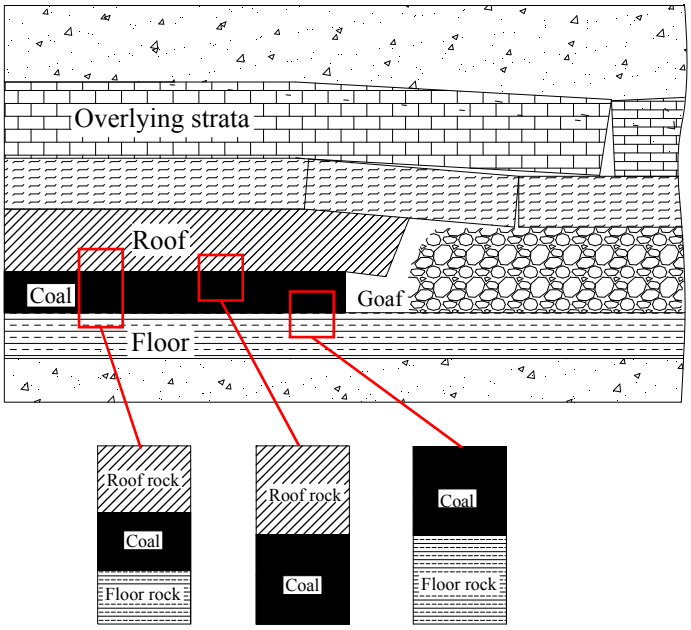

Fig. 1. Composite structures of rock and coal layers

(2018a). The effects of loading and unloading rates on the deformation and failure behaviors of a rock-coal-rock composite sample were studied (Huang & Liu, 2013). The precursory data of a sandstone-coal composite sample and a sandstone-coal-mudstone composite sample were studied by Zhao et al. (2008). Compared with a single coal sample, it is more difficult to predict the failure of a coal-rock composite sample. The failure characteristics and mechanical behavior of a rock-coal-rock composite sample with different strengths and stiffnesses were studied and analyzed (Zhao et al., 2014; Liu et al., 2015). Zuo et al. (2016) studied the failure behavior and strength characteristics of a coal-rock composite sample under different confining pressures. Using PFC software, the effects of the interface angel on the failure characteristics of a rock-coal composite sample were simulated and studied by Zhao et al. (2016). he rock burst trends of a roof rock-coal composite sample, a rock-coal-rock composite sample, and a coal-rock composite sample were studied (Liu et al., 2004). Besides, the characteristics of AE and electromagnetic radiation of composite samples subjected to different loads were analyzed (Rafael & Cristobal, 2010; Takeuchi et al., 2006).

These studies significantly contribute to the understanding of strength and failure characteristics of a composite structure of rock and coal layers. However, all of them focused on the intact composite sample of rock and coal. Rock and coal are natural materials formed by the aggregation of mineral particles and cement in a certain ratio under long-term geological effects. Generally, rock is relatively dense, and it has almost no macronative defects. Raw coal is relatively soft, and it has a significant amount of native defects such as joints, fractures, and various micro inclusions and pores, influencing the strength and failure characteristics of composite samples. The effects of native defects on the mechanical characteristics of pure coal or rock samples have been evaluated (Bobet, 2000; Kulatilake et al., 2011; Dyskin et al., 1994; Fujii & Ishijima, 2004;

Gholami & Rasouli, 2014; Tarokh et al., 2017; Kulatilake et al., 2001). However, composite samples of rock and raw coal with more complete and relatively original defects were selected for laboratory tests. Also, a complete and isotropic model of the composite sample of rock and coal was established for numerical simulation tests. Thus, the effects of native defects in coal on the strength and failure characteristics of composite samples are ignored. Yin et al. (2018b) analyzed the effects of joint angle in coal on the UCS of a roof rock-coal composite sample using PFC2D software. The results show that the joint in coal shows deterioration effects on the UCS, and with the increase in joint angle, the UCS of composite samples first decreased and then increased.

In this paper, the uniaxial compression simulation tests on the coal-rock composite sample with coal persistent joint were performed using PFC2D software. The effects of coal persistent joint on the strength and failure characteristics of the coal-rock composite materials were the main target of the investigation.

2. Numerical model of coal-rock composite sample

2.1. Partilcle flow code

Cundall and Strack (1979) established the particle flow theory based on the discrete element method. In the PFC2D software, the elements are mainly two-dimensional circular particles and walls, both of which are rigid and undeformable, while overlaps among elements are allowed as they contact each other. During the calculation loop process of PFC2D software, the contact, displacement and interaction among particles satisfy the Newton's second law and force–displacement law.

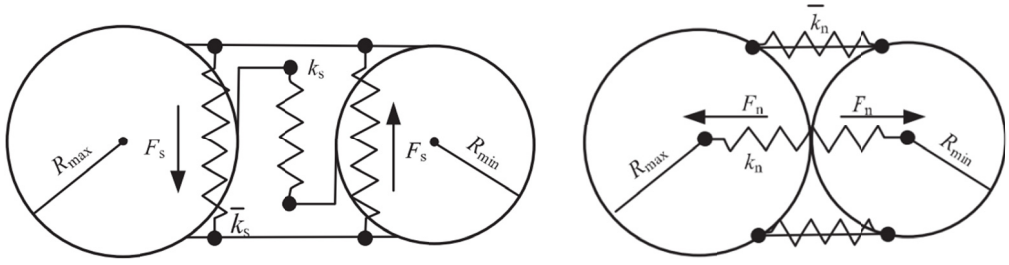

(a) Shear stiffness (b) Normal stiffness

Fig. 2. Sketch of parallel bond model (Itasca Consulting Group, 2008). k_n and k_s are the normal and shear stiffness of particles, respectively; R_{max} and R_{min} are the radii of larger and smaller particles of both contacting particles, respectively; F_n and F_s are the normal and shear contacting forces between particles, respectively; $\overline{k_n}$ and $\overline{k_s}$ are the normal and shear stiffness of parallel bonding particles, respectively

There are mainly two types of bond models in PFC2D software: contact bond model and parallel bond model. In the parallel bond model, a series of springs with constant normal and shear rigidity are evenly distributed on the contact surface with their contact points as the center, as shown in Fig. 2 (Itasca Consulting Group, 2008). Therefore, the relative motions at the contact points produce forces and bending moments; this is well applied to simulate compact materials

such as rock and coal (Lee & Jeon, 2011; Manouchehrian et al., 2014; Potyondy & Cundall, 2004). In this study, uniaxial compression models for coal-coal composite samples with a coal persistent joint were built using the parallel bond model.

2.2. Microparameters of coal and rock

In the parallel bond model, the macromechanical properties of rock and coal are mainly affected by the microparameters of particles in PFC2D software. The microparameters of rock and coal are determined by minimizing the error between simulation and experimental results. This is achieved by adjusting the microparameters to match the elastic modulus, Poisson's ratio, and peak stress of standard rock or coal specimen (a diameter of 50 mm and a height of 100 mm) provided by the laboratory test (Yin et al., 2018b). Due to the limitation of laboratory test conditions, the parameters of coal and rock provided by Zhao et al. (2016) were used to conduct numerical test.

TABLE 1

Microparameters of rock and coal (Zhao et al., 2016)

Parameters	Rock	Coal	Parameters	Rock	Coal
Minimum particle size [mm]	0.2		Parallel bond elastic modulus [GPa]	12	4
Particle size ratio	1.5		Parallel bond normal strength [MPa]	45	15
Density [kg/m^3]	2600	1800	Parallel bond tangential strength [MPa]	45	15
Contact modulus of the particle [GPa]	12	4	Parallel bond normal stiffness/ tangential stiffness	2.5	
Parallel bond radius multiplier	1		Normal stiffness/tangential stiffness	2.5	
Coefficient of friction	0.5				

2.3. Numerical model construction

In this study, the rock and coal freely overlap in a composite sample and the contact surface is the bedding plane without cohesive force. A uniaxial compression model for the coal-rock composite sample with coal persistent joint was established and generated by radius extension, as shown in Fig. 3. The length and height of the model are 50 mm and 100 mm, respectively. To evaluate conveniently, the height ratio of coal to rock was set as 1:1. A total of 21390 particles were generated in the model. The bedding plane and coal persistent joint plane were generated by JSET command. The origin of coal persistent joint is in the coal center. To facilitate the distinction, the particles through the bedding plane are colored in blue and the particles through the joint plane are colored in red. The wall is lengthened appropriately for preventing the spill-out of the particles.

According to various studies on jointed rock mass, the microparameters of the bedding plane and coal persistent joint plane are weakened and set as very small values (Yin et al., 2018b; Park & Song, 2009; Kulatilake et al., 2001). In this study, the friction coefficients of the bedding plane and coal persistent joint plane were set as 0.1, and their parallel bond compressive strengths and parallel bond cohesive strengths were all set as 0.

Now, the coal–rock composite sample model with a coal persistent joint was well built. In order to evaluate the effects of the coal persistent joint on the strength and failure characteristics

of composite samples, the included angles α between the persistent joint and loading direction were taken as 0°, 15°, 30°, 45°, 60°, 75°, and 90°. The loading was performed by moving the upper wall at a loading rate of 0.05 m/s.

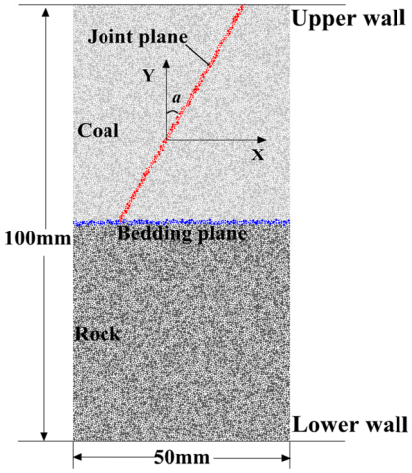

Fig. 3. Numerical model for coal-rock composite sample with a coal persistent joint

3. Strength characteristics of coal-rock composite sample with coal persistent joint

3.1. Effects of coal persistent joint on the strength of coal-rock composite sample

The simulation results of UCS, peak strains and elastic moduli of composite samples are shown in Table 2. Fig. 4 shows the uniaxial compression stress-strain curves of the coal-rock composite samples. Fig. 5 shows the variation trends of UCS and peak strain with the change in α.

TABLE 2

Numerical simulation results of coal-rock composite samples under uniaxial loading

Category	UCS [MPa]	Elastic modulus [GPa]	Peak strain [%]
Intact composite sample	23.816	7.996	0.30762
$\alpha = 0°$	23.637	7.970	0.30704
$\alpha = 15°$	19.621	7.836	0.26822
$\alpha = 30°$	14.467	7.693	0.23545
$\alpha = 45°$	14.872	7.796	0.19797
$\alpha = 60°$	22.688	7.932	0.2975
$\alpha = 75°$	23.37	7.948	0.30452
$\alpha = 90°$	22.33	7.949	0.30473

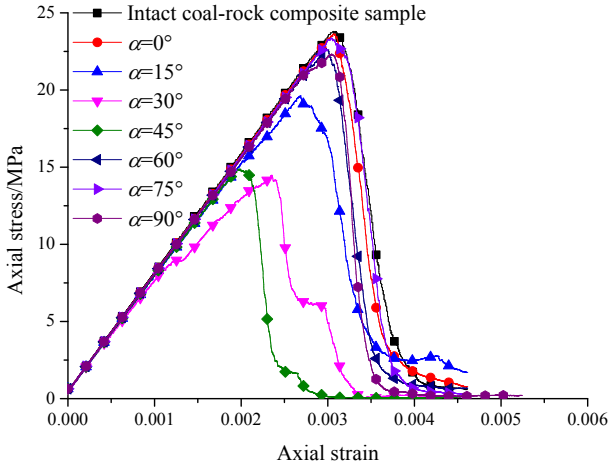

Fig. 4. Uniaxial compression stress-strain curves of coal-rock composite samples

In Fig. 4 shows that the complete stress-strain curves of coal-rock composite samples with a coal persistent joint are quite similar, basically consistent with that of intact coal-rock composite sample. The stress-strain curve generally can be divided into four stages: linear elastic deformation stage, nonlinear deformation stage, post-peak strain softening stage, and residual strength stage. The coal persistent joint does not affect the trend of stress-strain curve, but it affects the strain required for each stage. No obvious change was observed for the elastic modulus with the change in α, indicating that the stress-strain curves coincide at the linear elastic deformation stage, as also shown in Table 2: The elastic modulus slightly varies with the increase in α. The coal persistent joint affects the UCS and peak strain of composite samples. Because of the differences in α, the effects are different, which were quantitatively analyzed as follows:

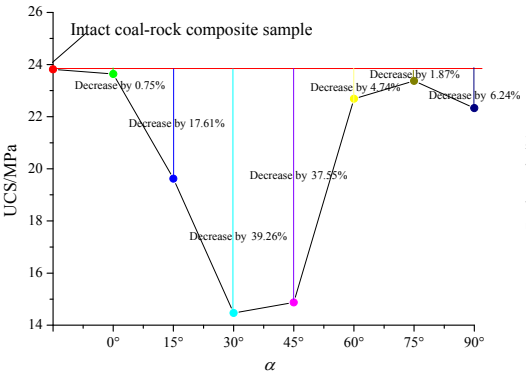

(a) Relationship between the UCS and α

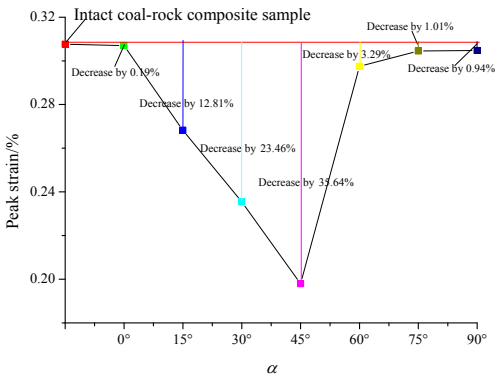

(b) Relationship between the peak strain and α

Fig. 5. Relationships between UCS, peak strain, and α

In Fig. 5, with the increase in α, the UCS and peak strain first decrease and then increase, consistent with that of single jointed rock mass (Huang and Yang, 2015). When α is 0°, 60°, 75°, and 90°, compared with the intact composite sample, UCS decreases by 0.75%, 4.74%, 1.87%, and 6.24%, respectively. The corresponding peak strains decrease by 0.19%, 3.29%, 1.01%, and 0.94%, respectively. The UCS and peak strains of composite samples with a coal persistent joint slightly differ from those of intact composite sample, indicating that the coal persistent joint within the abovementioned range of α slightly affects the UCS and peak strains of composite samples. However, when α is between 15° and 45°, compared with the intact composite sample, UCS values decrease by 17.61%, 39.26%, and 37.55%, respectively. The homologous peak strains decrease by 12.81%, 23.46%, and 35.64%, respectively. The UCS and peak strains of composite samples with a coal persistent joint are much less than those of intact composite sample, indicating that the coal persistent joint within the abovementioned range of α slightly affects the UCS and peak strains of composite samples.

3.2. Strength of coal-rock composite sample with a coal persistent joint

The structural plane in rock mass severely affects the rock mass strength, and the strength of rock mass with a structural plane is closely related to the corresponding failure pattern (Kulatilake et al., 2001; Liang et al., 2012; Cao et al., 2016). When a rock mass undergoes fracture failure along the structural plane, the corresponding strength is the lowest. When α is 0°, 15°, 60°, 75°, and 90°, the shear failure crossing the coal persistent joint plane within coal mainly causes the instability and failure of composite samples, consistent with the intact composite sample. The loadings are carried by the intact parts of coal and rock. Thus, the corresponding strengths are relatively large. Additionally, when α is 30°, the instability and failure of composite sample are caused by the combined effects of shear failure along the coal persistent joint plane within coal and tensile failure within rock. The loadings are carried by the coal persistent joint plane and intact parts of coal and rock. Thus, the strength is relatively small. The shear failure along the coal persistent joint plane within coal causes the instability and failure of composite sample at α of 45°. The loadings are mainly carried by the coal persistent joint. Thus, the strength is the lowest.

Additionally, the macrofracture failure of rock materials reflects the formation, propagation, and coalescence of microcracks in specimens. According to Section 4.1, the microcrack number shows a steep upward trend in the vicinity of peak stress or peak stain, indicating a rapid formation, propagation, and coalescence of microcracks. Then, they form a macrofailure crack and cause the instability and failure of composite samples. When the stress intensity transmitted between the particles is larger than the parallel bonding forces between the particles, microcracks can be generated. Fig. 6 shows the parallel bonding forces between the particles of composite samples at the peak stress stage. With the increase in α, the parallel bonding force between particles first decreases and then increases. The parallel bonding force at α of 45° is the lowest. Thus, the stress intensity transmitted between particles required for crack initiation first decreases and then increases. Macroscopically, the strength of composite sample first decreases and then increases, and the strength at α of 45° is the lowest.

However, in this study, UCS is the lowest at α of 30°. UCS at α of 45° has the second lowest value. This is because of the following: In PFC2D, the axial stress of composite samples indicates the average stress of upper wall. Fig. 7 shows the movement trend and failure model of composite

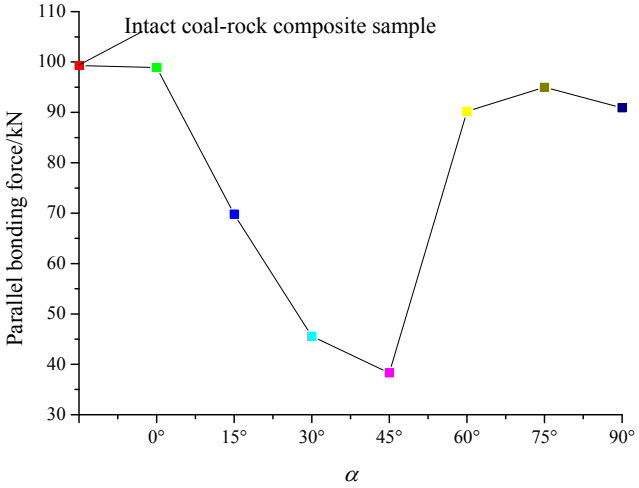

Fig. 6. Parallel bonding forces of composite samples at the peak stress stage

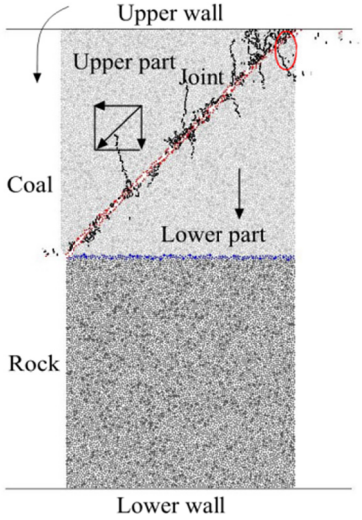

Fig. 7. Movement tendency and failure model of composite sample at α of 45°

sample at α of 45°. Taking the coal persistent joint plane as the boundary, the composite sample can be divided into two parts: upper part and lower part. In Fig. 7, the black line with arrowheads presents the movement tendency of different parts of composite sample. Because the fracture failure along the coal persistent joint plane occurs at α of 45°, the upper part movement can be divided into horizontal and vertical direction motion, and the lower part movement is the vertical direction motion. Owing to the unconformity of upper and lower parts, the upper wall has a trend of counterclockwise deflection. In PFC2D, the movement was set in the vertical direction, and deflection cannot occur. Thus, stress is concentrated at the top region of lower part of composite

sample (red circle area in Fig. 7). After destruction, the particles at the top region were severely destroyed, and they spill out. Therefore, the local stress concentration may enhance the average stress of upper wall and then increase the UCS at α of 45°.

4. Failure characteristics of coal-rock composite sample with a coal persistent joint

4.1. Microcrack number evolution

Fig. 8 shows the microcrack number evolution curves of composites samples. With the increase in axial strain, the microcrack number evolution trends of composite samples with a coal persistent joint are quite similar, basically consistent with that of intact composite sample, which can be divided into four stages: no microcrack stage, slow growth stage, rapid growth stage, stable stage. In the vicinity of peak strain of composite samples, the microcrack number has a steep upward trend, indicating a rapid formation, propagation, and coalescence of microcracks to form macrofailure cracks. This causes the instability and failure of composite samples. Fig. 8 shows that axial strains corresponding to the occurrence of a steep upward trend in the microcrack number of composite samples with a coal persistent joint are less than that of intact composite sample, especially at α of 30° and 45°. This indicates that the coal persistent joint enhances the transformation from unstable crack expansion to the macro-instability of composite samples. When α is 30° or 45°, because of both the shear failure along the persistent joint within coal and tensile failure within rock, the transformations from unstable crack expansion to macro-instability are rapid.

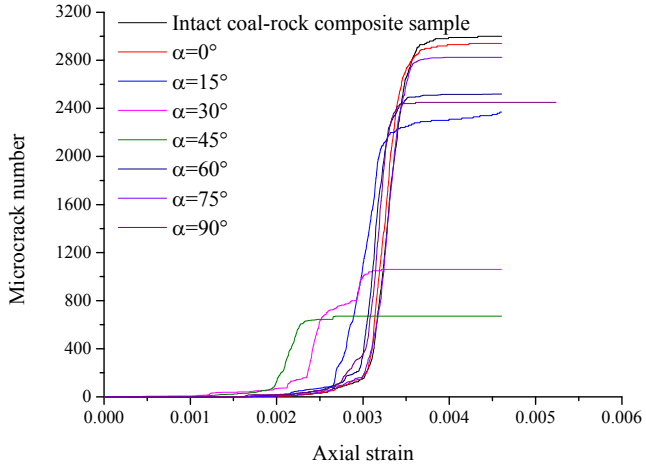

Fig. 8. Microcrack number evolution curves of composites samples

Taking the composite sample at α of 0° as an example, the microcrack number evolution of a composite sample was analyzed, as shown in Fig. 9.

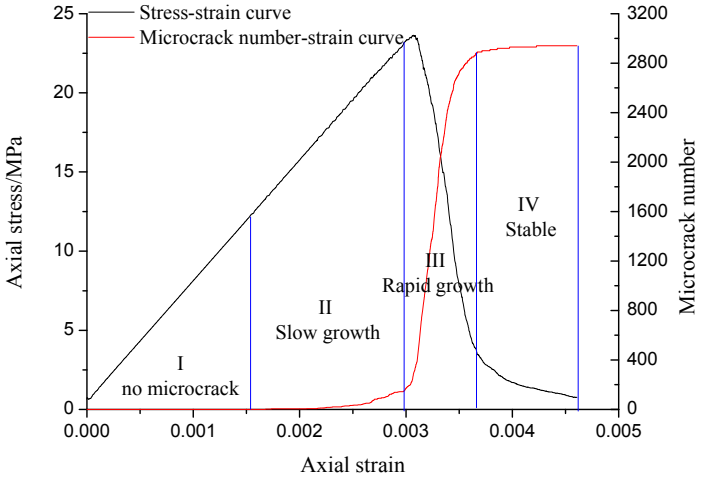

Fig. 9. Microcrack number evolution of the composites sample at α of 0°

At the initial stage of loading, the stress intensity transmitted between particles is less than the bonding strength between particles. Thus, no microcrack is generated at this stage. With the increase in axial stress, when the stress intensity transmitted between particles is larger than the bonding strength between particles, the first microcrack is generated. Then, with the further increase in axial stress, the composite sample changes from linear elastic deformation stage to nonlinear deformation stage. A few microcracks are generated, showing a slow growth of microcrack number in Fig. 9. When the axial stress further increases, more microcracks are generated, and propagation and coalescence occur, showing a steep upward trend of microcrack number in Fig. 9. Now, the microcracks change from stable propagation stage to unstable propagation stage. The macrofailure plane is formed in the composite sample. Finally, in the residual deformation stage, the composite samples mainly slip along the macrofailure plane (noncoal persistent joint plane), or the sliding along the coal persistent joint plane tends to be stable. A small number of microcracks are still generated. The microcrack number tends to be stable.

4.2. Failure patterns of composite samples

Fig. 10 shows the failure patterns of composite samples. When α values are 0°, 45°, 60°, 75°, and 90°, the failures of composite samples mainly occur within the coal, and no apparent destruction is observed for rock. However, when α is 90°, the rock near the bedding plane is destroyed by crack propagation in coal. Both the rock and coal of composite samples at α of 15° and 30° are destroyed; especially, an obvious tensile failure is observed for the rock at α of 30°.

The coal persistent joint affects the failure pattern of composite samples. The intact composite sample mainly undergoes shear failure within the coal. The coalescence of main failure plane and secondary failure planes makes the composite sample more broken. Fig. 11 shows the maximum microcrack number of composite samples after failure. The maximum microcrack number of intact composite samples after failure is 2998. When α is 0°, 15°, 60°, 75°, and 90°, the composite samples undergo shear failure crossing the coal persistent joint plane, basically consistent with

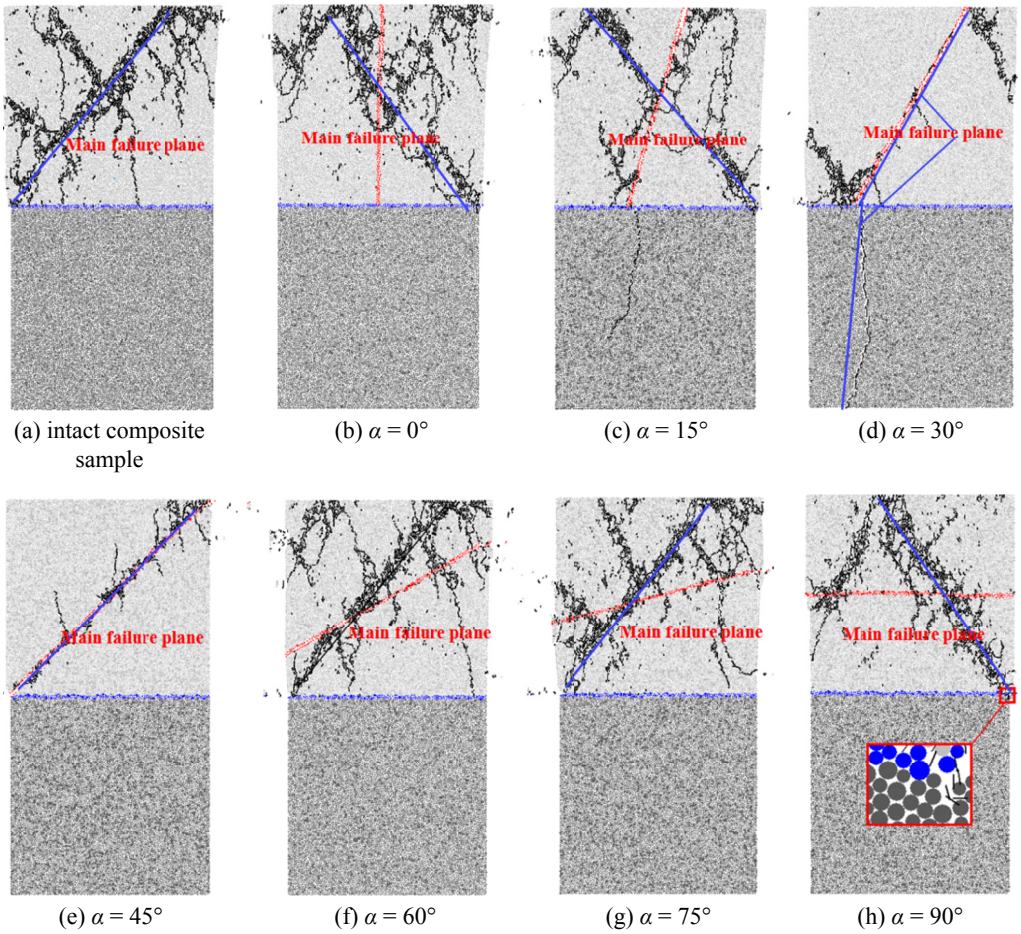

(a) intact composite sample (b) $\alpha = 0°$ (c) $\alpha = 15°$ (d) $\alpha = 30°$

(e) $\alpha = 45°$ (f) $\alpha = 60°$ (g) $\alpha = 75°$ (h) $\alpha = 90°$

Fig. 10. Failure patterns of composite samples

that of intact composite sample. When α is 15°, the microcrack propagation forms a small tensile crack in the rock body. The maximum microcrack numbers of composite samples after failure are 2942, 2370, 2519, 2824, and 2450, respectively. Compared with the intact composite sample, they decrease by 1.87%, 20.95%, 15.98%, 5.80%, and 18.28%, respectively. However, the shear failure along the coal persistent joint in coal and tensile failure in rock occur in the composite sample at α of 30°. The fragmentation degree is significantly reduced. After failure, there are 1060 microcracks, decreasing by 64.64% compared with the intact composite sample. The shear failure along the coal persistent joint causes the instability and failure of composite sample at α of 45°. The composite sample can be divided into two parts with the lowest fragmentation degree after failure. Compared with the intact composite sample, the maximum microcrack number after failure decreases up to 77.62%.

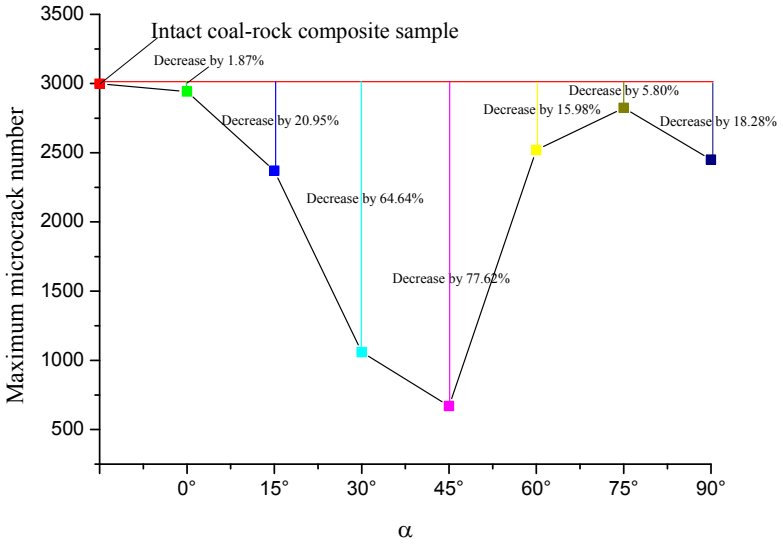

Fig. 11. Maximum microcrack numbers of composite samples after failure

5. Conclusions

In this study, the coal-rock composite samples with a coal persistent joint and a height ratio of 1:1 were established using the parallel bond model in PFC2D software. The rock and coal freely overlapped into a composite sample. The uniaxial compression tests on composite samples were simulated, and the effects of coal persistent joint on the strength and failure characteristics of composite samples were studied. The main conclusions are as follows:

(1) The UCS and peak strains of coal-rock composite sample with a coal persistent joint are less than those of the intact composite sample. While, the elastic modulus is close to that of the intact composite sample. The UCS and peak strains at α of 0°, 60°, 75°, and 90° slightly differ from those of intact composite sample.

(2) With the increase in α from 0° to 90°, the UCS and peak strain of composite samples first decrease and then increase. The peak strain at α of 45° is the lowest. The UCS at α of 30° is the smallest, inconsistent with the theoretical analysis of lowest UCS at α of 45°. This is because the local stress concentration caused by the inconformity of composite samples may enhance the average stress of upper wall and then increase the UCS of composite sample.

(3) The coal persistent joint enhances the transformation from unstable crack expansion to macro-instability of composite samples. The failures of most composite samples mainly occur within the coal, and no apparent destruction is observed for rock. Among them, the shear failure crossing the coal persistent joint plane mainly occurs at α of 0°, 15°, 60°, 75°, and 90°, and the shear failure along the coal persistent joint occurs at α of 45°. When α is 15°, the microcrack propagation induces a small tensile failure of rock. The shear failure along the coal persistent joint in coal and tensile failure in rock cause the instability and failure of composite sample at α of 30°.

Acknowledgments

This work was supported by National Natural Science Foundation of China (51904167, 51474134, 51774194, 51874189), Taishan Scholars Project, Taishan Scholar Talent Team Support Plan for Advantaged & Unique Discipline Areas, SDUST Research Fund, Shandong Provincial Natural Science Fund for Distinguished Young Scholars (JQ201612), Shandong Provincial Key Research and Development Plane (2017GSF17112).

References

Bao C.Y., Tang C.A., Cai M., Tang S.B., 2013. *Spacing and failure mechanism of edge fracture in two-layered materials*. International Journal of Fracture **181**, 2, 241-255.

Cao R.H., Cao P., Lin H., Pu C.J., Ou K., 2016. *Mechanical behavior of brittle rock-like specimens with pre-existing fissures under uniaxial loading, experimental studies and particle mechanics approach.* Rock Mechanics and Rock Engineering **49**, 3, 763-783.

Chen S.J., Yin D.W., Jiang N., Wang F., Guo W.J., 2019. *Simulation study on effects of loading rate on uniaxial compression failure of composite rock-coal layer*. Geomechanics and Engineering **17**, 4, 333-342.

Chen S.J., Yin D.W., Zhang B.L., Ma H.F., Liu X.Q., 2017. *Study on mechanical characteristics and progressive failure mechanism of roof-coal pillar structure body.* Chinese Journal of Rock Mechanics and Engineering **37**, 7, 1588-1598.

Cundall P.A., Strack, O.D.L., 1979. *A discreate numerical model for granular assemblies*. *Géotechnique* **29**, 1, 47-65.

Espinoza D.N., Pereira J.M., Vandamme M., Dangla P., Vidal-Gilbert S., 2015. *Desorption-induced shear failure of coal bed seams during gas depletion*. International Journal of Coal Geology **137**, 142-151.

Gholami R., Rasouli V., 2014. *Mechanical and elastic properties of transversely isotropic slate*. Rock Mechanics and Rock Engineering **47**, 5, 1763-1773.

Huang B.X., Liu J.W., 2013. *The effect of loading rate on the behavior of samples composed of coal and rock.* International Journal of Rock Mechanics and Mining Sciences **61**, 23-30.

Hauquin T., Gunzburger Y., Deck O., 2018. *Predicting pillar burst by an explicit modelling of kinetic energy*. International Journal of Rock Mechanics and Mining Sciences **107**, 159-171.

Itasca Consulting Group. 2008. *PFC2D (Particle Flow Code in 2 Dimensions) Fish in PFC2D*. Itasca Consulting Group, Minneapolis, Minn, USA.

Huang Y.H., Yang S.Q., 2015. *Discrete element study on strength and failure behavior of jointed sandstone with two sets of cross-joints*. Journal of China Coal Society **40**, S1, 76-84.

Kulatilake P.H.S.W., Malama B., Wang J., 2001. *Physical and particle flow modeling of jointed rock block behavior under uniaxial loading*. International Journal of Rock Mechanics and Mining Sciences **38**, 5, 641-6579.

Lama R.D., Bodziony J., 1998. *Management of outburst in underground coal mines*. International Journal of Coal Geology **35**, 1-4, 83-115.

Lee H., Jeon S., 2011. *An experimental and numerical study of fracture coalescence in pre-cracked specimens under uniaxial compression*. International Journal of Solids and Structures **48**, 6, 979-999.

Li X.B., Feng F., Li D.Y., Du K., Ranjith P.G., Rostami J., 2018. *Failure characteristics of granite influenced by sample height-to-width ratios and intermediate principal stress under true-triaxial unloading conditions*. Rock Mechanics and Rock Engineering **51**, 5, 1321-1345.

Liang Z.Z., Xing H., Wang S.Y., Williams D.J., Tang C.A., 2012. *A three-dimensional numerical investigation of the fracture of rock specimens containing a pre-existing surface flaw*. Computers and Geotechnics **45**, 19-33.

Liu B., Yang R.H., Guo D.M., Zhang D.Z., 2004. *Burst-prone experiments of coal-rock combination at -1000 m level in Suncun coal mine.* Chinese Journal of Rock Mechanics and Engineering **23**, 14, 2402-2408.

Liu J., Wang E.Y., Song D.Z., Wang S.H., Niu Y., 2015. *Effect of rock strength on failure mode and mechanical behavior of composite samples*. Arabian Journal of Geosciences **8**, 7, 4527-4539.

Liu Q., Nie W., Hua Y., Peng H.T., Liu C.Q., Wei C.H. 2019. *Research on tunnel ventilation systems:dust diffusion and pollution behaviour by air curtains based on CFD technology and field measurement*. Building and Environment. **147**, 444-460.

Lu C.P., Liu G.J., Liu Y., Zhang N., Xue J.H., Zhang L., 2015. *Microseismic multi-parameter characteristics of rock-burst hazard induced by hard roof fall and high stress concentration.* International Journal of Rock Mechanics and Mining Sciences **76**, 18-32.

Manouchehrian A., Sharifzadeh M., Marji M.F., Gholamnejad J., 2014. *A bonded particle model for analysis of the flaw orientation effect on crack propagation mechanism in brittle materials under compression*. Archives of Civil and Mechanical Engineering **14**, 1, 40-52.

Park J.W., Song J.J., 2009. *Numerical simulation of a direct shear test on a rock joint using a bonded-particle model.* International Journal of Rock Mechanics and Mining Sciences **46**, 8, 1315-1328.

Paul A., Singh A.P., John L.P., Singh A.K., Khandelwal M., 2012. *Validation of RMR-based support designusingroof bolts by numerical modeling for undergroundcoal mine of Monnet Ispat, Raigarh, India-a case study*. Arabian Journal of Geosciences **5**, 6, 1435-1448.

Petukhov I.M., Linkov A.M., 1979. *The theory of post-failure deformations and the problem of stability in rock mechanics.* International Journal of Rock Mechanics and Mining Science and Geomechanics Abstracts **16**, 2, 57-76.

Poulsen B.A., Shen B., Williams D.J., Huddlestone-Holmes C., Erarslan N., Qin J., 2014. *Strength reduction on saturation of coal and coal measures rocks with implications for coal pillar strength.* International Journal of Rock Mechanics and Mining Science **71**, 41-52.

Potyondy D.O., Cundall P.A., 2004. *A bonded-particle model for rock.* International Journal of Rock Mechanics and Mining Science **41**, 8, 1329-1364.

Rafael R., Cristobal L., 2010. *Analysis of methane emissions in a tunnel excavated through Carboniferous strata based on underground coal mining experience*. Tunnelling and underground space technology **25**, 4, 456-468.

Snelling P.E., Godin L., McKinnon S.D., 2013. *The role of geologic structure and stress in triggering remote seismicity in Creighton Mine, Sudbury, Canada.* International Journal of Rock Mechanics and Mining Science **58**, 166-179.

Takeuchi A., Laub W.S., Freund F.T., 2006. *Current and surface potential induced by stress-activated positive holes in igneous rocks*. Physics and Chemistry of the Earth **31**, 4-9, 240-247.

Tarokh A., Makhnenko R.Y., Fakhimi A., Labuz J.F., 2017. *Scaling of the fracture process zone in rock.* International Journal of Fracture **204**, 2, 191-204.

Yin D.W., Chen S.J., Xing W.B., Huang D.M., Liu, X.Q., 2018a. *Experimental study on mechanical behavior of roof-coal pillar structure body under different loading rates*. Journal of China Coal Society **43**, 5, 1249-1257.

Yin D.W., Chen S.J., Liu X.Q., Ma H.F., 2018b. *Effect of joint angle in coal on failure mechanical behavior of rock-coal combined body.* Quarterly Journal of Engineering Geology and Hydrogeology **51**, 2, 202-209.

Zhao T.B., Guo W.Y., Lu C.P., Zhao G.M., 2016. *Failure characteristics of combined coal-rock with different interfacial angles.* Geomechanics and Engineering **11**, 3, 345-359.

Zhao Y.H., Jiang Y.D., Zhu J., Sun G.Z., 2008. *Experimental study on precursory information of deformation of coal-rock composite sample before failure.* Chinese Journal of Rock Mechanics and Engineering **27**, 2, 339-346.

Zhao Z.H., Wang W.M., Dai C.Q. Yan J.X., 2014. *Failure characteristics of three-body model composed of rock and coal with different strength and stiffness.* Transactions of Nonferrous Metals Society of China **24**, 5, 1538-1546.

Zuo J.P., Chen Y., Zhang J.W., Wang J.T., Sun Y.J., Jiang G.H., 2016. *Failure behavior and strength characteristics of coal-rock combined body under different confining pressures.* Journal of China Coal Society **41**, 11, 2706-2713.